Real-time observation of dendrite coarsening in Sn-13%Bi alloy by synchrotron microradiography

B. Li,[1] H. D. Brody,[1] and A. Kazimirov[2]
[1]*Department of Materials Science and Engineering, University of Connecticut, Storrs, Connecticut 06269-3136, USA*
[2]*Cornell High Energy Synchrotron Source, Ithaca, New York 14853, USA*
(Received 24 June 2004; published 16 December 2004)

An improved synchrotron microradiography technique is being used to study dendrite growth and coarsening in Sn-13%Bi alloy in real time. The morphology of growing dendrites can be well resolved with reasonable image contrast. Dendrite arm remelting, coalescence, and fragmentation have been observed in a real alloy and in real time during solidification under controlled thermal gradients and cooling rates. This research opens a different window to the study of alloy solidification and enables unambiguous understanding of solidification processes in optically opaque, metallic alloys.

DOI: 10.1103/PhysRevE.70.062602 PACS number(s): 68.70.+w, 07.85.Qe, 64.70.Dv, 81.30.Fb

When alloys are solidified from liquid, the solid phase, mainly, takes a branched, dendritic morphology [1]. The length scale of the dendritic structure in alloys influences directly the mechanical behavior of materials in subsequent processing and in service. Dendrite morphology continually evolves during solidification, in particular, dendrite arm spacing increases. Several coarsening mechanisms have been proposed [2–4]. However, direct observations of dendrite arm coarsening during alloy solidification have not been recorded, mainly because metals are optically opaque.

Most studies of alloy solidification have relied on post-solidification analyses, i.e., morphological observations and compositional measurements on sectioned metallographic samples after completed or interrupted solidification [2,4–8]. Other investigators have observed solidification *in situ* in metals by looking at the surface of a solidifying sample [9,10]. Still, the evolution of structure inside the melt could not be seen. These indirect experimental observations have provided valuable insights toward understanding alloy solidification. Detailed quantitative data on transitions in dendrite morphologies during solidification are invisible to observations by optical techniques.

To circumvent the difficulties in directly observing dendrite growth in metals and alloys, materials scientists have been observing solidification in optically transparent materials [3,11–13]. Due to the significant difference in thermal and physical properties between metallic alloys and analog alloys, the mechanisms and kinetics of solidification processes may be different. For instance, the difference in thermal diffusivity between these two categories of materials is as much as three orders of magnitude.

The high penetrating power of x rays has made radiography techniques unique in viewing the internal structure of opaque materials, especially metals. With the availability of modern x-ray techniques, especially solid-state detectors, researchers have been exploring possibilities of applying radiographic techniques to the study of alloy solidification [14–17]. Only limited, qualitative results have been obtained, because of difficulties in experimentation. In this work, an improved x-ray microradiography technique has been used to observe in real time dendritic solidification in Sn-13%Bi alloy.

When x rays pass through a mixture of solid and liquid of a solidifying alloy sample, contrast is produced by differential absorption, which is mainly from solute partitioning during solidification. The difference in linear absorption coefficient between solid and liquid produces the contrast to distinguish the solid from the liquid. As shown in Fig. 1, image contrast, characterized by the ratio of intensities of the transmitted beams, $I_2/I_1 = e^{-(\mu_S - \mu_L)\cdot t_S}$ depends upon the thickness of the solid phase (t_S) and the absolute difference between the linear absorption coefficients (μ_L and μ_S). For Sn and Bi alloys, at Mo $K\alpha$ (17.44 KeV), $\mu_{s_n} = 243$ cm, $\mu_{B_i} = 1421$ cm. The large difference helps produce good image contrast.

An x-ray energy (about 20 KeV) between the two absorption edges of Sn and Bi is selected so that optimal image contrast can be achieved. Sn and Bi form eutectic alloys. During solidification the liquid is enriched in bismuth because of solute partitioning (partition ratio 0.368), and is increasingly absorptive. Additionally, the low liquidus temperature of this alloy makes it easier to fabricate a solidification apparatus. In this work, a relatively high composition (13%Bi) is selected.

Ideally the resolution of solid-state detectors such as image intensifiers and fluorescent crystals is on the order of a few microns. This capacity cannot be fully achieved when imaging alloy solidification. As shown in Fig. 1, resolution of the position of the solid liquid interface, for example, depends on the dynamic range of the detector; the divergence of the x-ray beam; and the rate of movement of the interface.

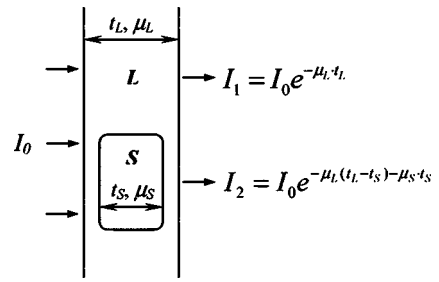

FIG. 1. Contrast produced by differential absorption between solid (S) and liquid (L) when x rays pass through a mushy zone. I is intensity, μ linear absorption coefficient, and t thickness.

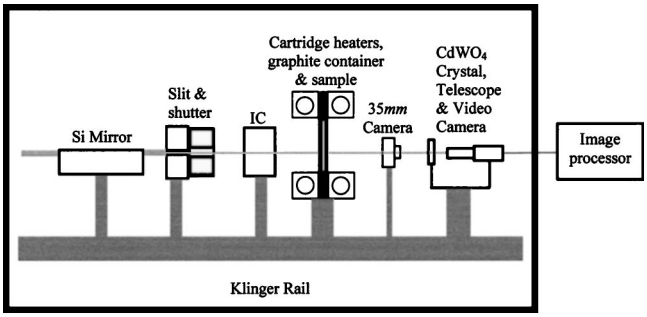

FIG. 2. Synchrotron x-ray imaging setup for real time microradiography used at hutch A2 of CHESS.

In this work, a $CdWO_4$ fluorescent crystal and high resolving power negative film (320 line pairs) are being used together to capture moving dendrites. Compared with solid-state detectors, negative emulsions have slow response to x-ray photons but higher spatial resolution and contrast. In addition, the full size of the beam can be used for imaging on film.

A high intensity (typically 200 mA ring current, photon flux $6\times10^{10}\mathrm{cm}^2$ sec) parallel x-ray beam from synchrotron radiation at the Cornell High Energy Synchrotron Source (CHESS) has been used for imaging. A parallel beam helps eliminate the penumbral (geometric) unsharpness produced by a divergent beam emitted from a conventional source. The problem of slow response of negative film to x rays can be overcome with the high intensity. Exposure times for a 100–150-μm-thick sample can be reduced to 0.1 sec or even shorter.

A special solidification furnace contains the sample and provides the desired temperature control. A thin (typically 130 μm in thickness), well-polished solid sample is sandwiched and sealed between two graphite plates. Graphite is almost transparent to x rays, little attenuation occurs when x rays pass through the graphite crucible. Cooling rate (ϵ) and temperature gradient (G) in the sample can be controlled independently. For the temperature controls in this work, the growth rate of dendrites ranges from 10 to 30 μm/sec, thus dynamic dendrite growth can be recorded with negligible image blurring.

Experiments of synchrotron microradiography are performed at Hutch A2 of CHESS. The experimental setup is shown, schematically, in Fig. 2 The shape of the incident x-ray beam is defined by a slit. A rhodium/gold coated silicon mirror is installed to filter high-energy harmonics (60 KeV) of the beam and to reflect the 20-KeV photons to the sample. Separation of the high-energy component from the desired monochromatic 20-KeV beam is critical, because the high-energy harmonics produce undesired exposure. The ion chamber (IC) converts photon signals into electrical pulses (counts), such that the shutter and photon flux can be controlled electronically. A video system comprised of a $CdWO_4$ crystal, telescope, and charge-coupled device is used to observe dendrite growth in real time but with low resolution. As soon as the growing dendrites come into the field of view, the 35-mm camera is started to capture higher quality images. The camera is remotely controlled by a timer and advances film a desired distance for each shot. Positive images are developed and then digitized by a high-resolution scanner without any subsequent, undue image processing.

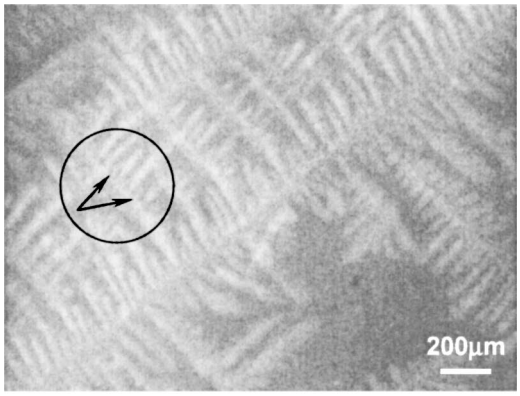

(a) Growing dendrites

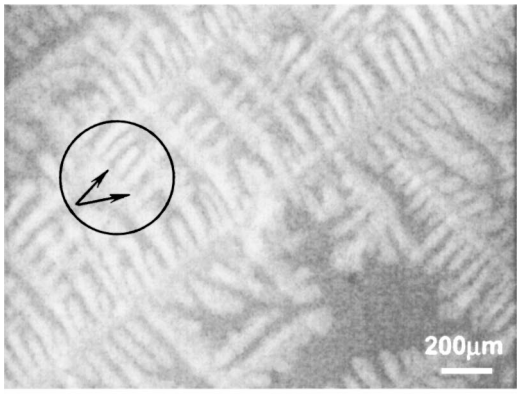

(b) 120 seconds from (a)

FIG. 3. Dendrite coarsening by remelting from tip toward root of small dendrite arms (designated by arrows) during continuous cooling. Cooling rate $\epsilon=8.3\times10^{-3}$ K/s. Temperature gradient $G\approx0$.

The x-ray beam is focused on the sample near the top thermocouple. Changes in dendrite morphologies with time in that area can be recorded as the sample is either cooled continuously through the freezing range or held at a constant temperature. Animations made up of the captured individual images in time sequence allow us to track changes in morphology in the irradiated area.

Figures 3–5 present images of growing dendrites during solidification. The sample shown in Figs. 3 and 4 was heated above the liquidus temperature, cooled at a rate of 8.3×10^{-3} K/s with a negligible temperature gradient, and then held isothermally at 484 K.

The images shown in Fig. 3, taken during the cooling stage, illustrate dendrite coarsening by remelting of small dendrite arms. The small dendrites, indicated by arrows in the encircled regions, remelted from their tips toward their roots, and disappeared. This coarsening mechanism was also observed at faster cooling rates. Small dendrite branches disappeared quickly in the early stage of continuous cooling.

The images shown in Fig. 4, taken while the sample was held isothermally at 484 K, show a different dendrite coars-

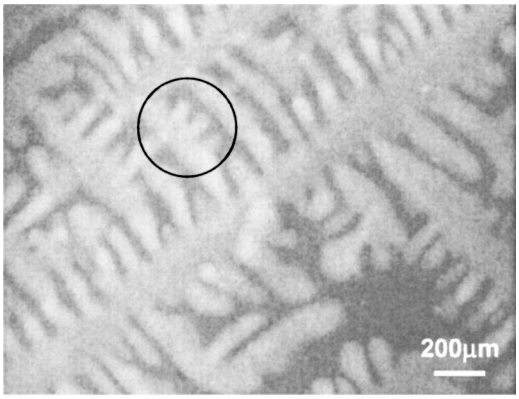

(a) Held at 484*K* for 960 seconds

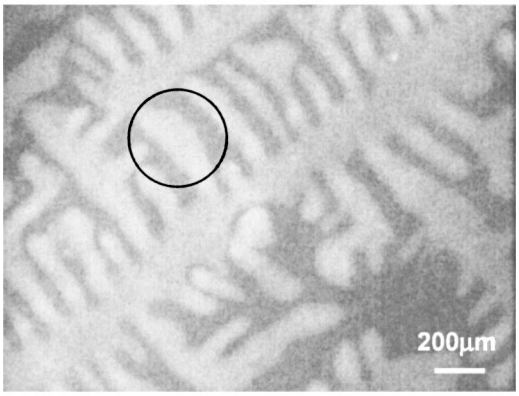

(b) Held at 484*K* for 2040 seconds

FIG. 4. Dendrite coarsening by coalescence during an isothermal hold at 484 K. Liquid grooves between the three encircled dendrite arms were filled by local solidification. Negligible gradient.

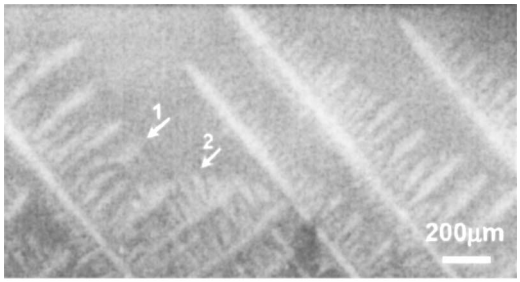

(a)

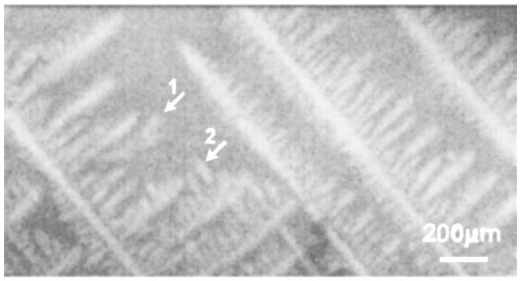

(b)

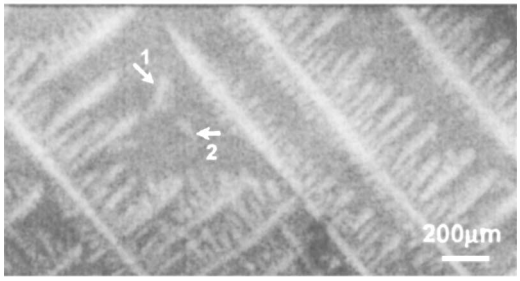

(c)

FIG. 5. Fragmentation observed during directional solidification. Time interval between the images shown is 40 sec. The dendrite fragments, indicated by arrows, are lighter than the bismuth enriched-liquid and float upward. Cooling rate $\epsilon = 3.3 \times 10^{-2}$ K/s, $G = 1.3$ K/mm.

ening mechanism. Interdendritic liquid regions between neighboring branches were replaced by localized solidification from the dendrite roots toward the dendrite tips.

The microradiographs shown in Fig. 5, taken while the sample was melted and directionally solidified at a cooling rate of 3.3×10^{-2} K/s and a temperature gradient of 1.3 K/mm, show dendrite fragmentation. A secondary and a tertiary arm, indicated by arrows, separated near their roots and floated upward. The tin rich solid is less dense than the interdendritic liquid, which is enriched in bismuth. The fragments were trapped in liquid pools. Dendrite fragmentation was observed only sporadically during directional solidification with a finite gradient G; and no dendrite fragmentation was observed during solidification under a negligible temperature gradient.

In our observations, the dendrite growth is confined within a thin liquid wall. The effect of convection is minimized. Thus the coarsening is predominantly surface tension driven and diffusion controlled. Because the diffusion distance is on the same order of the dendrite arm spacing, the real time observations in this work could provide interesting insight about dendrite coarsening.

The three mechanisms of dendrite coarsening illustrated in Figs. 3–5, dendrite remelting, coalescence, and fragmentation contribute to the increase of dendrite arm spacing. The driving force for dendrite coarsening is reduction in solid-liquid interfacial energy. In accordance with the Gibbs-Thomson effect, the composition of liquid in equilibrium with a solid phase is a function of local curvature of the liquid-solid interface. The concentration gradient established between locations with a difference in local curvature gives rise to diffusive mass transfer through the interdendritic liquid, and the resultant dendrite remelting, coalescence and fragmentation. Beyond these general theories, what actually happened to dendrites growing in liquid could not be revealed in the past due to the opacity of alloys.

An improved synchrotron microradiography technique is being applied to the study in real time of dendrite growth and coarsening in Sn-13%Bi alloy. Coarsening mechanisms such as dendrite arm remelting from tips to roots, coalescence by

local solidification at liquid grooves between side arms, and fragmentation have been observed. This technique can be used to study solidification in real alloys in real time and to provide clarifications to mechanisms of alloy solidification.

This work is based upon research conducted at the Cornell High Energy Synchrotron Source (CHESS), which is supported by the National Science Foundation and the National Institutes of Health/National Institute of General Medical Sciences under Grant No. DMR 9713424. The authors gratefully acknowledge the continued support of the Office of the Provost of the University of Connecticut. The authors thank Professor J. E. Morral, Professor T. Z. Kattamis, Professor D. M. Pease, Professor E. H. Jordan of the University of Connecticut, and W. J. Boettinger of the National Institute for Standards and Technology (NIST) for their insightful comments and suggestions. Special thanks are extended to Dr. Dingfei Zhang, currently at the University of Chongqing, People's Republic of China, for his assistance with the experiments.

[1] J. S. Langer, Science **243**, 1150 (1989).
[2] T. Z. Kattamis, J. C. Coughlin, and M. C. Flemings, Trans. Soc. Min. Eng. AIME **239**, 1504 (1967).
[3] M. Kahlweit, Scr. Metall. **2**, 251 (1968).
[4] K. P. Young and D. H. Kirkwood, Metall. Trans. A **6A**, 197 (1975).
[5] J. J. Reeves and T. Z. Kattamis, Scr. Metall. **5**, 223 (1971).
[6] N. J. Whisler and T. Z. Kattamis, J. Cryst. Growth **15**, 20 (1972).
[7] S. K. Kailasam, M. E. Glicksman, S. S. Mani, and V. E. Fradkov, Metall. Mater. Trans. A **30A**, 1541 (1999).
[8] S. P. Marsh and M. E. Glicksman, Metall. Mater. Trans. A **27A**, 557 (1996).
[9] M. E. Glicksman and R. J. Schaefer, Acta Metall. **14**, 1126 (1966).
[10] R. J. Schaefer and M. E. Glicksman, Trans. Soc. Min. Eng. AIME **239**, 257 (1967).
[11] K. A. Jackson and J. D. Hunt, Acta Metall. **13**, 1212 (1965).
[12] K. A. Jackson, J. D. Hunt, D. R. Uhlmann, and T. P. Seward, Trans. Soc. Min. Eng. AIME **236**, 149 (1966).
[13] C. A. Norlund and R. Trivedi, Metall. Mater. Trans. A **31A**, 1261 (1998).
[14] P. A. Curreri and W. F. Kaukler, Metall. Mater. Trans. A **27A**, 801 (1996).
[15] S. Sen, W. F. Kaukler, P. Curreri, and D. M. Stefanescu, Metall. Mater. Trans. A **28A**, 2129 (1997).
[16] R. H. Mathiesen, L. Arnberg, F. Mo, T. Weitkamp, and A. Snigirev, Phys. Rev. Lett. **83**, 5062 (1999).
[17] H. N. Thi *et al.*, J. Phys. D **36**, A83 (2003).